

Elastic Scattering and Total Reaction Cross Section for the ${}^6\text{He} + {}^{27}\text{Al}$ System

E. A. Benjamim¹, A. Lépine-Szily¹, D. R. Mendes Junior¹, R. Lichtenthäler¹,
V. Guimarães¹, P. R. S. Gomes², L. C. Chamon¹, M. S. Hussein¹, A. M. Moro³,
A. Arazi⁴, I. Padron^{2,5}, J. Alcantara Nuñez¹, M. Assunção¹, A. Barioni¹,
O. Camargo Jr.¹, R. Z. Denke¹, P. N. de Faria¹, K. C. C. Pires¹

¹ *Instituto de Física - Universidade de São Paulo, C.P.66318,05389-970 São Paulo, Brazil*

² *Instituto de Física - Universidade Federal Fluminense, Niterói, R.J., 24210-340, Brazil*

³ *Departamento de FAMN, Universidad de Sevilla, Apdo 1065, E-41080, Sevilla, Spain*

⁴ *Laboratorio Tandem, Departamento de Física, Comisión Nacional de Energía*

Atómica, Av. del Libertador 8250, (1429), Buenos Aires, Argentina

⁵ *CEADEN, P.O. Box 6122, Havana, Cuba*

September 13, 2018

Abstract

The elastic scattering of the radioactive halo nucleus ${}^6\text{He}$ on ${}^{27}\text{Al}$ target was measured at four energies close to the Coulomb barrier using the RIBRAS (Radioactive Ion Beams in Brazil) facility. The São Paulo Potential (SPP) was used and its diffuseness and imaginary strength were adjusted to fit the elastic scattering angular distributions. Reaction cross-sections were extracted from the optical model fits. The reduced reaction cross-sections of ${}^6\text{He}$ on ${}^{27}\text{Al}$ are similar to those for stable, weakly bound projectiles as ${}^6,7\text{Li}$, ${}^9\text{Be}$ and larger than stable, tightly bound projectile as ${}^{16}\text{O}$ on ${}^{27}\text{Al}$.

Reactions induced by halo nuclei are currently one of the main subjects in Nuclear Physics, with interest in nuclear structure, reactions, astrophysics and production of superheavy elements. Nowadays reliable measurements of elastic, inelastic and transfer cross sections of unstable projectiles are possible due to new Radioactive Nuclear Beam (RNB) facilities. Nuclei that have small separation energies have large probability of breaking-up when the colliding nuclei approach each other. In this case their interactions convert potential and kinetic energy into relative kinetic energy between their fragments. Many efforts have been made, both theoretical and experimental, to investigate the effect of the break-up on the fusion cross section [1]. However most of the experiments in the field of fusion have been carried out with intense beams of stable weakly bound nuclei (${}^6\text{Li}$, ${}^7\text{Li}$, ${}^9\text{Be}$), which have respectively separation energies of $S_\alpha=1.48$ MeV, $S_\alpha=2.45$ MeV and $S_n=1.67$ MeV, larger than those for halo radioactive nuclei. Nevertheless important features of the reactions induced by halo nuclei are not present in those reactions. As an example, we mention that halo nuclei have larger nuclear radii, which corresponds to a lowering of the Coulomb barrier. Also, important couplings to the soft dipole resonance that may be present in the case of halo nuclei with quite different proton and neutron distributions, do not occur for normal nuclei. For the 2 neutron halo nuclei with Borromean nature (while the 3 body (core + 2n) system is bound, any of the 2 body subsystems (core + 1n) or (2n) is unbound) the ${}^{11}\text{Li}$ and ${}^6\text{He}$ are good examples. The correlation between the 2 neutrons of the halo is also important feature as recent measurements on the Coulomb dissociation of ${}^{11}\text{Li}$ have demonstrated [2]. Strong low-energy (soft) E1 excitation was observed, peaked at about $E_x=0.6$ MeV with $B(E1)=1.42(18)$ e² fm². The spectrum is reproduced well by a three-body model with a strong two-neutron correlation. Similar features have been observed for other two-neutron Borromean nuclei ${}^6\text{He}$ [3] and ${}^{14}\text{Be}$ [4] and possibly for the two-proton Borromean nucleus ${}^{17}\text{Ne}$ [5]. Break-up effects are also expected to play an important role in the scattering mechanism, affecting the imaginary part of the interaction potential. So far, conflicting predictions have been made about whether the fusion of weakly bound nuclei is enhanced or hindered owing to the strong coupling

to the break-up channel [6, 7, 8, 9, 10, 11]. The role of the Coulomb and nuclear break-up and their interferences on the fusion process is a subject of great interest [9, 11, 12]. One of the important questions is whether the effect of the break-up is essentially to increase the total reaction cross section, instead of affecting the fusion cross section. Depending on whether the break-up is dominated by the Coulomb or nuclear interactions, different effects on the fusion cross section could result. Therefore, it is essential to investigate the dependence of the break-up and total reaction cross sections on the break-up threshold energy of different projectiles and on the target mass.

So far, reactions induced by halo nuclei have been studied mostly on heavy targets, such as ${}^6\text{He} + {}^{209}\text{Bi}$ [13, 14, 15], ${}^6\text{He} + {}^{238}\text{U}$ [16, 17], and ${}^{11}\text{Be} + {}^{209}\text{Bi}$ [18], although recently experiments have been performed with ${}^6\text{He}$ projectile on medium mass targets, namely ${}^{64}\text{Zn}$ [19] and ${}^{65}\text{Cu}$ [20]. For heavy systems, where the Coulomb break-up predominates, very large total reaction cross sections have been obtained at energies around and below the Coulomb barrier due to the intense long range Coulomb field. In this case the transfer + break-up cross sections were found to account for most of the total reaction cross section. For the medium mass targets, where the Coulomb field is not so intense, transfer and break-up cross sections were found to be much more important than the fusion cross section at energies above the Coulomb barrier and the total reaction cross sections were much larger than for ${}^4\text{He}$ or ${}^6\text{Li}$ projectiles [19, 20]. In a comparison between total reaction cross sections for ${}^6\text{He}$, ${}^6\text{Li}$, ${}^7\text{Li}$, ${}^9\text{Be}$, ${}^{16}\text{O}$ projectiles on ${}^{64}\text{Zn}$ target, Gomes et al [21] have shown that the reaction cross section is largest for the ${}^6\text{He}$ (halo nucleus with threshold energy of 0.975 MeV), followed by the group of the three stable weakly bound projectiles, and finally the tightly bound ${}^{16}\text{O}$ projectile produces the smallest total reaction cross section.

In this work we have investigated the behavior of the total reaction cross section of the ${}^6\text{He} + {}^{27}\text{Al}$ system, and compared it with the available data for the ${}^9\text{Be} + {}^{27}\text{Al}$ [22, 23], ${}^6\text{Li} + {}^{27}\text{Al}$, ${}^7\text{Li} + {}^{27}\text{Al}$ [24] and ${}^{16}\text{O} + {}^{27}\text{Al}$ systems [25]. For the ${}^6\text{He} + {}^{27}\text{Al}$ system the contribution from the nuclear break-up should be predominant not just due to the weaker Coulomb field, but also due to the long range nuclear interaction of the two neutron halo projectile ${}^6\text{He}$ with the target. For ${}^9\text{Be} + {}^{27}\text{Al}$, despite the relatively weak Coulomb field, it was observed [22] that the transfer plus break-up processes still have a significant cross section. The study of the elastic scattering and transfer + break-up processes for the ${}^{6,7}\text{Li} + {}^{28}\text{Si}$ systems [26] also shows the importance of the nuclear break-up process for stable weakly bound nuclei on a light mass target.

The study of light systems with very weakly bound and neutron rich exotic nuclei is particularly interesting, since there are reactions of great astrophysical interest involving these nuclei. As an example, in the case of inhomogeneous distribution of protons and neutrons following the Big Bang not only stable light elements but also proton and neutron rich short-lived elements such as ${}^6\text{He}$, ${}^7\text{Be}$, ${}^8\text{B}$ and ${}^8\text{Li}$ would be present in the early universe. These, short lived, radioactive nuclei could thus bridge the $A=8$ mass gap and heavier elements would then be synthesized. Reactions involving light unstable nuclei would be present also in the Type-II supernovae, neutron stars and in massive stars. Besides the triple alpha capture, the α -recombination and the bridge of mass 5 and 8 in the beginning of r-process in a Type-II supernova could be given via alternate three-body reactions or sequential capture reactions such as ${}^4\text{He}(2n,\gamma){}^6\text{He}(2n,\gamma){}^8\text{He}$ [27]. In this case, the two neutron capture reaction cross sections on ${}^4\text{He}$ and ${}^6\text{He}$ depend strongly on the pronounced halo structure of the ${}^6\text{He}$ and ${}^8\text{He}$ compound nuclei.

In a recent paper Milin et al. [28] have presented elastic and inelastic scattering as well as 2n transfer reaction angular distributions for the ${}^6\text{He} + {}^{12}\text{C}$ system, measured at $E_{lab} = 18$ MeV, which is well above the Coulomb barrier (3 MeV for the ${}^6\text{He} + {}^{12}\text{C}$ system). The main goal of their work was the spectroscopic investigation of stretched neutron configurations in the ${}^{14}\text{C}$ final nucleus.

This is the first paper reporting on experiments with radioactive beams using the recently installed RIBRAS facility, at São Paulo [29]. This facility is installed at the Pelletron Laboratory of the University of São Paulo and extends the capabilities of the original Pelletron Tandem Accelerator of 8MV terminal voltage (8UD) by producing secondary beams of unstable nuclei. The most important components of this facility are the two new superconducting solenoids with 6.5 T maximum central field and a 30 cm clear warm bore, which corresponds to a maximum angular acceptance in the range of $2 \text{ deg} \leq \theta \leq 15 \text{ deg}$. The solenoids are installed on the 45B beam line of the Pelletron Tandem. Thus the actual system is similar to the TWINSOL facility at Notre Dame University [30, 31]. The presence of the two magnets is very important to produce pure secondary beams. However in the present work only the first solenoid was

used. When using only one solenoid the secondary beam still has some contaminants easily identified in elastic scattering experiments.

The production system consists of a gas cell, mounted in a ISO chamber with a $2.2\mu\text{m}$ Havar entrance window and a ${}^9\text{Be}$ vacuum tight exit window $16\mu\text{m}$ thick, which plays the role of the primary target and the window of the gas cell at the same time. The gas inside the cell has the purpose of cooling the Berilium foil heated by the primary beam and can also be used as production target. A few centimeters behind the gas cell there is a tungsten rod of 2.4cm diameter with a cylindrical hole of 1cm diameter per 2cm length, to stop and collect the primary beam particles. In front of the W beam stopper there is a circular colimator which is polarized to a negative voltage of about -250 Volts in order to supress the secondary electrons emitted from the cup. The experimental set-up, with the production target, the W beam stopper, the magnets and the scattering chamber, with secondary target and detectors is presented in Fig. 1.

The ${}^6\text{He}$ secondary beam was produced by the ${}^9\text{Be}({}^7\text{Li}, {}^6\text{He}){}^{10}\text{B}$ reaction with $Q = -3.38$ MeV, by impinging about 300 nAe primary beam of ${}^7\text{Li}$ on the $16\mu\text{m}$ thick ${}^9\text{Be}$ production target. The primary beam is stopped in a Faraday cup, constituted by an isolated Tungsten rod which stops all particles in the angular region from 0 to 2 degrees and where the primary beam intensities were integrated. The reaction products of the secondary beam were detected using two $\Delta\text{E-E}$ Si telescopes, with detector thicknesses of $22\text{-}150\mu\text{m}$ and $50\text{-}150\mu\text{m}$ respectively, with antiscattering collimators separated by 4 cm in front of the ΔE detectors. The distance from the secondary target to the collimator, which limited the solid angle to 15 msr, was 8 cm and the angular opening of the collimators was about ± 2.6 degrees. The secondary beam was not pure, reminiscence of the primary beam was detected at zero degrees in the $2+$ charge state, as well as ${}^4\text{He}$, ${}^3\text{H}$ and protons were transmitted with the appropriate energy through the first solenoid. The secondary targets used in this experiment were a ${}^{27}\text{Al}$ target of 7.2 mg/cm^2 and a ${}^{197}\text{Au}$ target of 5 mg/cm^2 .

The secondary beam intensities were calculated by assuming pure Rutherford scattering of the ${}^6\text{He}$ on the gold target. From this intensity and from the integrated charge of the primary beam intensity for every run one can derive the production efficiency which is the ratio of secondary to primary beam intensities. As this efficiency does not depend on the target but only on the energy, it was used for the determination of the secondary beam intensities on Aluminum targets allowing the calculation of the absolute cross sections.

The effective solid angles and the average detection angles were determined by using a Monte Carlo simulation, which took into account the collimator size, the secondary beam spot size on the secondary target ($\phi=4\text{ mm}$), the secondary beam divergence (1.5-3.5 degrees, was limited by collimators following the primary target) and the angular distribution at forward angles in the detector, which modifies the average detection angles. The total angular uncertainty of ± 3.2 degrees was calculated with the Monte Carlo simulation and includes the beam spot size, the secondary beam divergence and angular straggling in the target.

We have used the primary ${}^7\text{Li}$ beam at the four different incident energies 19.0, 20.5, 21.0 and 22.0 MeV. The secondary beam energies were calculated by energy losses and confirmed by the energy measurement in the Si telescope, calibrated with alpha particles of a radioactive ${}^{241}\text{Am}$ source. The ${}^6\text{He}$ secondary beam energies in the middle of the ${}^{27}\text{Al}$ secondary target were respectively 9.5, 11.0, 12.0 and 13.4 MeV, while the value of the Coulomb barrier in the laboratory system for the ${}^6\text{He} + {}^{27}\text{Al}$ system is about 8.0 MeV. The total energy loss of the ${}^6\text{He}$ beam in the thick Al target is about 3.2 MeV. After passing through the thick ${}^{27}\text{Al}$ target, the ${}^6\text{He}$ beam has lost 1.6MeV on its way to the middle of the target and 1.6MeV on its way out. These energy losses also apply roughly for the scattered particles. The energy resolution is determined by three components: the energy resolution of the ${}^6\text{He}$ beam, the energy straggling in the target and the kinematical broadening of the scattered particles. The energy resolution (FWHM) with the thick Al target is the the full width of the elastic peak in the energy spectrum and its value is about 400 keV, thus sufficient to separate the inelastic excitation of the first excited state of ${}^{27}\text{Al}$ at 843 keV. The ${}^6\text{He}$ secondary beam intensity at these energies was about 0.7×10^5 pps/ $(\mu\text{Ae of } {}^7\text{Li})$.

The results for the angular distributions are shown in Fig. 2. The error bars in the cross sections of the angular distributions are due to the statistical errors. The error bars in the scattering angles are of ± 3.2 degrees and were calculated with the Monte Carlo simulation.

The elastic scattering cross sections of the angular distributions were reproduced by optical model

calculations obtained with the São Paulo Potential (SPP) [32, 33], which is a folding optical potential which takes nonlocal effects into account. The imaginary part of the potential has the same form factor as the real part and the only free parameters were the normalization of the imaginary potential, N_I and a , the diffuseness of the nuclear density of the projectile.

We have fitted the angular distributions by minimizing the χ^2 . In this procedure, N_I and a were varied, but we have assumed that a common diffuseness value should be assumed for all energies. The best value of the diffuseness was $a=0.56(2)$ fm. The best values N_I were 0.8(5), 0.8(4), 0.6(4) and 0.7(5) for the energies 9.5, 11.0, 12.0 and 13.4 MeV, respectively. The errors in the parameters are determined from the χ^2 parabola, at the value of $\chi^2 = \chi^2_{min} + 1$. The reaction cross sections were calculated using the best fit optical potentials, with the best common diffuseness $a = 0.56$ fm and the best value of N_I for each energy. Their uncertainty comes from the quoted uncertainties in the optical potential, namely in the diffuseness a and in the imaginary normalization factor N_I . The large error in the reaction cross sections (± 100 mb), comes mainly from the large error in the imaginary normalization factor N_I . If we use the best common N_I for all angular distributions, $N_I=0.65(20)$, the error in N_I is reduced. The best diffuseness, $a=0.56(2)$ fm corresponds to the diffuseness of the matter distribution of the ${}^6\text{He}$ nucleus and is the convolution of the point nucleon distribution of ${}^6\text{He}$ with the intrinsic matter distribution of the nucleon. From the deconvolution we obtained the diffuseness of the point nucleon distribution of ${}^6\text{He}$ as being 0.52(2) fm. This diffuseness is much larger than the diffuseness of ${}^4\text{He}$, which is about 0.3 fm, deduced in similar manner [36]. The ${}^6\text{He}$ density obtained in the present work is compatible with other experimental evidences [37, 36] and with theoretical calculations [34, 35].

For the other systems, as ${}^9\text{Be} + {}^{27}\text{Al}$ [22, 23], ${}^6\text{Li} + {}^{27}\text{Al}$, ${}^7\text{Li} + {}^{27}\text{Al}$ [24] and ${}^{16}\text{O} + {}^{27}\text{Al}$ [25], the elastic scattering angular distributions available were analysed using the same procedure employed for the ${}^6\text{He} + {}^{27}\text{Al}$ system. All elastic scattering angular distributions were fitted using the SPP, allowing for the variation of N_I and density diffuseness a . We have obtained different values of a for the different systems, as $a=0.53$ fm for the ${}^{16}\text{O}$, 0.56 fm for the ${}^7\text{Li}$, and 0.58 fm for the ${}^6\text{Li}$ and ${}^9\text{Be}$. All systems were analysed using the same procedure for consistency. All reaction cross sections were obtained from the fit of the elastic scattering angular distributions with SPP. The reaction cross sections determined in this way are presented in the Table I.

In order to compare total reaction cross sections for different systems we used the procedure suggested in ref [38], where the cross sections are divided by $(A_p^{1/3} + A_T^{1/3})^2$ and the center of mass energy by $Z_p Z_T / (A_p^{1/3} + A_T^{1/3})$, where Z_p (Z_T) and A_p (A_T) are the charge and mass of the projectile (target), respectively. In this way, the geometrical effects are removed and the eventual anomalous values of the reduced radii r_0 , which should be related to the physical processes to be investigated, are not washed out.

Figure 3 shows the results of the reduced total reaction cross sections, σ_R^{red} , for the halo ${}^6\text{He}$, the stable weakly bound ${}^9\text{Be}$, ${}^6,7\text{Li}$ and the tightly bound ${}^{16}\text{O}$ projectiles on the same ${}^{27}\text{Al}$ target. One can observe that the smallest cross section is for the tightly bound projectile ${}^{16}\text{O} + {}^{27}\text{Al}$, for which the break-up process is not expected to occur. The values of σ_R^{red} for the weakly bound stable nuclei on ${}^{27}\text{Al}$ are similar to each other and are larger than that for the ${}^{16}\text{O}$. Their uncertainties are of the order of 2-4%, due to the difference in the reaction cross section when different potentials are used, which give very similar quality in the fits. The values of σ_R^{red} for the halo nucleus ${}^6\text{He}$, which has the smallest break-up threshold energy and has the largest uncertainties, is seemingly similar to σ_R^{red} of the weakly bound stable nuclei. However the relation employed to obtain σ_R^{red} is entirely based on the use of the radius to mass number relation, $R = r_0 A^{1/3}$, which is not quite appropriate for halo nuclei such as ${}^6\text{He}$.

We have estimated the nuclear break-up cross-section by extending the closed formalism of Frahn for heavy ion inelastic scattering [39], based on the adiabatic Austern-Blair theory [40], to the break-up case by considering the latter as directly related to the multipole polarizability of the weakly bound nucleus [41]. If only dipole and quadrupole terms are considered we find,

$$\sigma_{break-up} \cong \left[(\delta_1)^2 \left(\frac{3}{2} \frac{\Delta R}{R} \right)^2 + (\delta_2)^2 \right] \sum_l (2l+1) \left| \frac{dS_N(l)}{dl} \right|^2 \quad (1)$$

where, $S_N(l)$ are the scattering matrix elements of the ${}^6\text{He}+{}^{27}\text{Al}$ collision calculated with the best fit optical potential, δ_i is the i^{th} multipole deformation length and $\Delta R \equiv R_n - R_p$ is the difference in the neutron and proton rms radii, while R is the rms matter radius. For ${}^6\text{He}$, $\Delta R = 0.61 \pm 0.21$ fm and $R =$

2.3 ± 0.07 fm [37]. In obtaining Eq.(1) we have ignored in the dipole contribution a term proportional to $d^2 S_N(l)/dl^2$. The dipole, δ_1 , and quadrupole, δ_2 , deformation lengths were deduced in [3] to be roughly equal and given by $\delta_1 \sim \delta_2 = 1.8$ fm. Our estimate, based on Eq.(1), of the nuclear break-up cross section for ${}^6\text{He} + {}^{27}\text{Al}$ is about 150 mb at $E_{lab} = 10$ MeV, of which the dipole contributions is about 30 mb while the contribution of the quadrupole is 120 mb. The estimate of $\sigma_{break-up}$ above does not include the Coulomb break-up which, if added, would give rise to a larger total break-up cross-section. Preliminary CDCC calculations [42] where the two halo neutrons in ${}^6\text{He}$ are treated as one dineutron entity, give very similar numbers as Eq.(1). The quadrupole deformation lengths of ${}^6\text{Li}$, ${}^7\text{Li}$ and ${}^9\text{Be}$ were calculated from their quadrupole moments [43] and nuclear rms matter radii [44] and their values are respectively 0.014, 0.73 and 0.70 fm. The dipole deformation of the ${}^6\text{Li}$, in the α -d cluster model is zero. Thus the nuclear break-up cross sections, calculated by Eq. 1, of the weakly bound ${}^6\text{Li}$, ${}^7\text{Li}$ and ${}^9\text{Be}$ nuclei on ${}^{27}\text{Al}$ are not more than 20% of the corresponding break-up cross section for the ${}^6\text{He} + {}^{27}\text{Al}$ system.

Equation (1) was derived assuming the validity of the adiabatic approximation, where the Q-value is ignored. This is the basis of the Austern-Blair formula. It should give an upper limit to the cross section. It is true that the Austern-Blair theory was originally employed for inelastic excitations of collective states. We do not see any reason why not using it for break-up considered as inelastic excitation into the continuum through dipole, quadrupole, etc, transitions. The nuclear break-up cross sections of ${}^6\text{Li}$, ${}^7\text{Li}$ and ${}^9\text{Be}$, obtained with Eq. (1) are less than 20% of that of ${}^6\text{He}$. This is a correct statement since the deformation lengths are much smaller and, further, the Q-values, not included in Eq. (1) are larger.

In summary, we report in this Letter the first results obtained with the new radioactive beam facility RIBRAS at São Paulo, with the measurement of elastic scattering between ${}^6\text{He}$ and the light ${}^{27}\text{Al}$ target, at four energies slightly above the Coulomb barrier. The derived total reaction cross sections were compared with other systems, the stable weakly bound ${}^9\text{Be}$, ${}^{6,7}\text{Li}$ and the tightly bound ${}^{16}\text{O}$ projectiles on the same target. The reduced reaction cross sections for the 2 neutron Borromean halo nucleus ${}^6\text{He}$ on ${}^{27}\text{Al}$ are similar to other weakly bound stable systems within the error bars. This indicates that for light systems the effects of the halo on the reaction cross sections could be much smaller than the effect observed in heavier systems. Certainly higher quality data are needed to observe the effect of the Borromean nature of ${}^6\text{He}$ on the reaction cross section at low energies.

Acknowledgements

The authors wish to thank the Fundação de Amparo à Pesquisa do Estado de São Paulo (FAPESP) and the Conselho Nacional de Desenvolvimento Científico e Tecnológico (CNPq) for financial support (FAPESP 2001/06676-9 and 2003/10099-2).

References

- [1] L.F. Canto *et al.*, Phys. Rep. **424**, 1 (2006).
- [2] T. Nakamura *et al.*, Phys. Rev. Lett. **96**, 252502 (2006).
- [3] T. Aumann *et al.*, Phys. Rev. C **59**, 1252 (1999).
- [4] M. Labiche *et al.*, Phys. Rev. Lett. **86**, 600 (2001).
- [5] R. Kanungo *et al.*, Phys. Lett. B **571**, (2003) 21.
- [6] M.S. Hussein *et al.*, Phys. Rev. C **46**, 377 (1992).
- [7] N. Takigawa *et al.*, Phys. Rev. C **47**, R2470 (1993).
- [8] C. H. Dasso, A. Vitturi, Phys. Rev. C **50**, R12 (1994).
- [9] L. F. Canto *et al.*, Phys. Rev. C **52**, R2848 (1995), Nucl. Phys. **A589**, 117 (1995).
- [10] K. Hagino *et al.*, Phys. Rev. C **61**, 037602 (2000).

- [11] A. Diaz-Torres, I. J. Thompson, Phys. Rev. C **65**, 024606 (2002).
- [12] V. Guimarães *et al.*, Phys. Rev. Lett. **84**, 1862 (2000).
- [13] E.F. Aguilera *et al.*, Phys. Rev. Lett. **84**, 5058 (2000); Phys. Rev. C **63**, 061603(R) (2001).
- [14] J.J. Kolata *et al.*, Phys. Rev. Lett. **81**, 4580 (1998).
- [15] P.A. De Young *et al.*, Phys. Rev. C **71**, 051601(R) (2005).
- [16] M. Trotta *et al.*, Phys. Rev. Lett. **84**, 2342 (2000).
- [17] R. Raabe *et al.*, Nature **431**, 823 (2004).
- [18] C. Signorini *et al.*, Europ. Phys. Journ. A **5**, 7 (1999).
- [19] A. Di Pietro *et al.*, Europhysics Letters **64**, 309 (2003); Phys. Rev. C **69**, 044613 (2004).
- [20] A. Navin *et al.*, Phys. Rev. C **70**, 044601 (2004).
- [21] P.R.S. Gomes *et al.*, Phys. Lett. B **601**, 20 (2004).
- [22] G. V. Marti *et al.*, Phys. Rev. C **71**, 027602 (2005).
- [23] P. R. S. Gomes *et al.*, Phys. Rev. C **70**, 054605 (2004).
- [24] J. M. Figueira *et al.*, Phys. Rev. C **73**, 054603 (2006).
- [25] E. Crema, Masters degree thesis USP, 1979 , unpublished
- [26] A. Pakou *et al.*, Phys. Rev. Lett **90**, 202701 (2003); Phys. Lett B **556**, 21 (2003); Phys. Rev. C **69**, 054602 (2004); Phys. Rev. C **71**, 064602 (2005).
- [27] J. Görres *et al.*, Phys. Rev. C **52**, 2231 (1995).
- [28] M. Milin *et al.*, Nucl. Phys. **A730**, 285 (2004).
- [29] R. Lichtenthäler *et al.*, Eur. Phys. J. A **25**,s01,733 (2005); Nucl. Phys. News **15** (3), 25 (2005).
- [30] J.J.Kolata *et al.*, Nucl. Instr. Meth. B **40/41**, 503 (1989).
- [31] F. D. Becchetti *et al.*, Nucl. Instrum. and Meth. in Phys. Res. A **505**, 377 (2003).
- [32] L. C. Chamon *et al.*, Phys. Rev. C **66**, 014610 (2002).
- [33] M.A. G. Alvarez *et al.*, Nucl. Phys. **A723**, 93 (2003).
- [34] M. V. Zhukov *et al.*, Nucl. Phys. **A552**, 353 (1993).
- [35] J. S. Al-Khalili *et al.*, Phys. Rev. C **54**, 1843 (1996).
- [36] L. R. Gasques *et al.*, Phys. Rev. C **67**, 024602 (2003); Phys. Rev. C **67**, 067603 (2003).
- [37] G. D. Alkhazov, *et al.*, Phys. Rev. Lett. **78**, 2313 (1997).
- [38] P. R. S. Gomes *et al.*, Phys. Rev. C **71**, 017601 (2005).
- [39] W. E. Frahn, Nucl. Phys. **A272**, 413 (1976).
- [40] N. Austern and J.S.Blair, Annals of Physics **33**, 15 (1965).
- [41] M. S. Hussein, to be published.
- [42] A.M. Moro, *et al.*, to be published.
- [43] P. Raghavan, Atomic Data and Nucl. Data Tables **42**(2), 189 (1989).
- [44] I. Tanihata, *et al.*, Phys. Rev. Lett. **55**, 2676 (1985).

System	E_{lab}	σ_R (mb)	E_{cm}^{red}	σ_B^{red}
${}^6\text{He} + {}^{27}\text{Al}$	9.5	1110(90)	1.44	48(4)
	11.0	1257(100)	1.67	54(4)
	12.0	1300(100)	1.82	56(4)
	13.4	1390(100)	2.03	60(4)
${}^6\text{Li} + {}^{27}\text{Al}$	7.0	113(3)	0.71	5(1)
	8.0	320(19)	0.81	14(1)
	10.0	625(4)	1.01	27(2)
	12.0	913(55)	1.21	39(2)
${}^7\text{Li} + {}^{27}\text{Al}$	6.0	51(2)	0.60	0.52(6)
	7.0	153(4)	0.70	2.10(6)
	8.0	226(7)	0.80	9.4(3)
	9.0	364(11)	0.90	15.1(4)
	10.0	536(16)	1.00	22.0(7)
	11.0	728(22)	1.10	30.2(9)
	12.0	840(25)	1.20	35(1)
	14.0	1055(32)	1.40	44(1)
	16.0	1240(37)	1.60	51(2)
	18.0	1294(39)	1.80	54(2)
${}^9\text{Be} + {}^{27}\text{Al}$	12.0	380(11)	0.88	14.7(4)
	14.0	583(35)	1.03	23(1)
	18.0	950(57)	1.32	37(2)
	22.0	1250(75)	1.61	48(2)
	25.0	1400(84)	1.83	54(2)
	28.0	1520(46)	2.05	59(2)
${}^{16}\text{O} + {}^{27}\text{Al}$	30.0	428(8)	1.00	14.0(3)
	35.0	678(13)	1.17	22.3(4)
	40.0	831(17)	1.33	27.3(5)
	45.0	979(20)	1.50	32.1(6)
	45.6	994(20)	1.52	32.6(6)

Table I. The reaction cross sections were obtained from the fit of the elastic scattering angular distributions of all systems with the São Paulo Potential (SPP) as explained in the text.

Figure 1: The experimental set-up, with the production target, the W beam stopper, the magnets and the scattering chamber, with secondary target and detectors. See text for details.

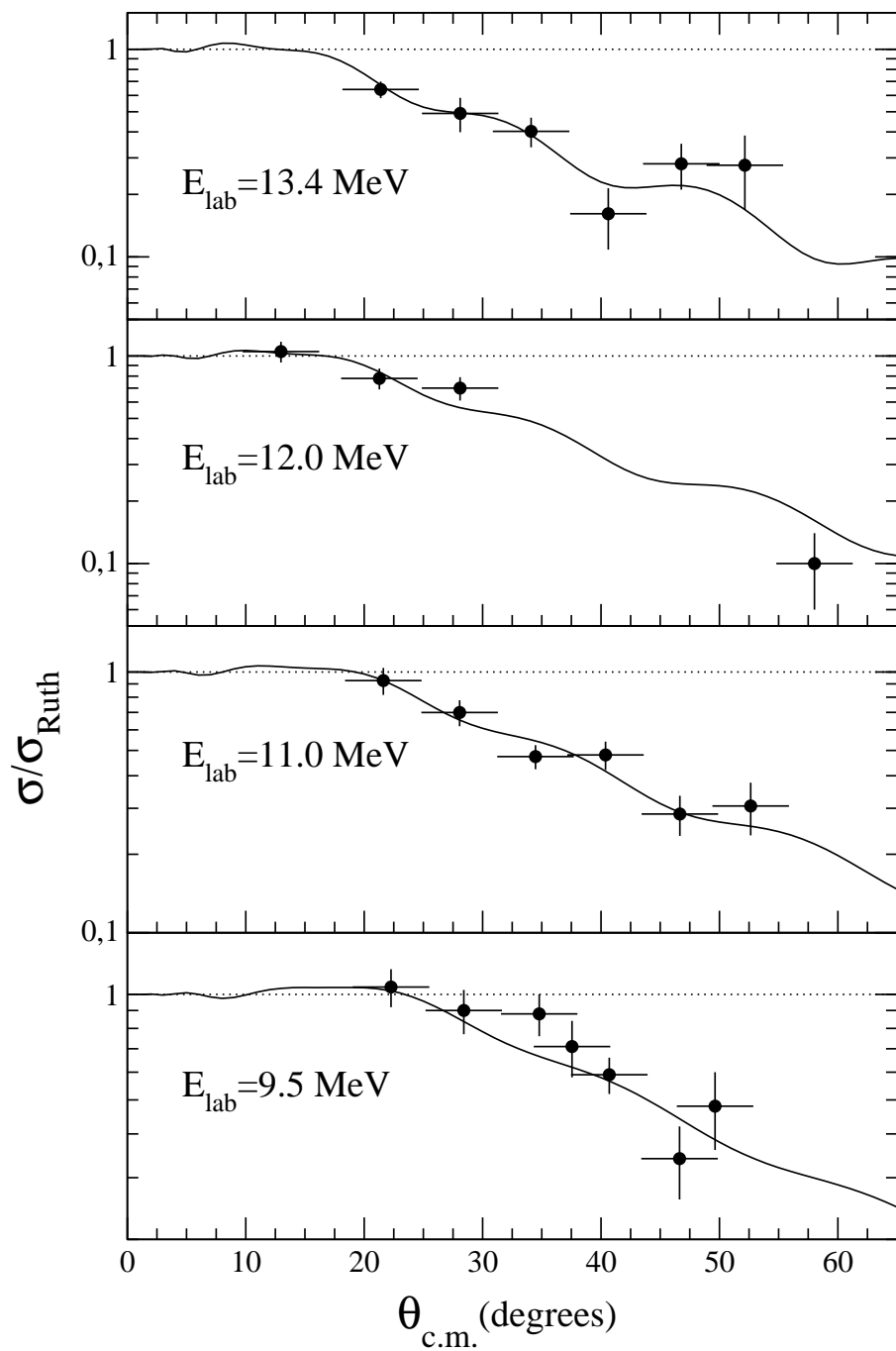


Figure 2: The elastic scattering angular distributions measured for the $^6\text{He} + ^{27}\text{Al}$ system together with best fits obtained with the SP potential (SPP). The diffuseness of the matter density used in the SPP was $a=0.56$ fm.

Figure 3: The reduced reaction cross sections for the ${}^6\text{He}+{}^{27}\text{Al}$ system obtained in this work together with reduced reaction cross sections of some weakly bound stable projectiles and of ${}^{16}\text{O}$ on ${}^{27}\text{Al}$.

